THE JOURNAL OF PHYSICAL CHEMISTRY A

Article

Cite This: J. Phys. Chem. A XXXX, XXX, XXX−XXX

pubs.acs.org/JPCA

Production of Br_2 from N_2O_5 and Br^- in Salty and Surfactant-Coated Water Microjets

Thomas B. Sobyra, Helena Pliszka, Timothy H. Bertram,* and Gilbert M. Nathanson*

Department of Chemistry, University of Wisconsin−Madison, 1101 University Avenue, Madison, Wisconsin 53706, United States

Supporting Information

ABSTRACT: Gas−liquid scattering experiments are used to investigate the oxidation−reduction reaction $N_2O_5(g) + 2Br^-(aq) \rightarrow Br_2(g) + NO_3^-(aq) + NO_2^-(aq)$, a model for the nighttime absorption of N_2O_5 into aerosol droplets containing halide ions. The detection of evaporating Br_2 molecules provides our first observation of a gaseous reaction product generated by a water microjet in vacuum. N_2O_5 molecules are directed at a 35 μm diameter jet of 6 or 8 *m* LiBr in water at 263 or 240 K, followed by detection of both unreacted N_2O_5 and product Br_2 molecules by velocity-resolved mass spectrometry. The N_2O_5 reaction probability at near-thermal collision energy is too small to be measured and likely lies below 0.2. However, the evaporating Br_2 product can be detected and controlled by the presence of surfactants. The addition of 0.02 *m* 1-butanol, which creates ∼40% of a compact monolayer, reduces Br_2 production by 35%. Following earlier studies, this reduction may be attributed to surface butanol molecules that block N_2O_5 entry or alter the near-surface distribution of Br^-. Remarkably, addition of the cationic surfactant tetrabutylammonium bromide (TBABr) at 0.005 *m* (9% of a monolayer) reduces the Br_2 signal by 85%, and a 0.050 *m* solution (58% of a monolayer) causes the Br_2 signal to disappear entirely. A detailed analysis suggests that TBA^+ efficiently suppresses Br_2 evaporation because it tightly bonds to the Br_3^- intermediate formed in the highly concentrated Br^- solution and thereby hinders the rapid release and evaporation of Br_2.

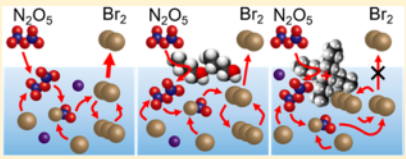

INTRODUCTION

Liquid microjets provide the opportunity to explore interactions between gases and aqueous solutions in vacuum with minimal interference from gas−water vapor collisions.[1−7] These narrow and fast-moving streams of water have diameters small enough to limit the density of the vapor cloud surrounding the jet, and they move fast enough to be observable before the jet breaks up into droplets and freezes. Among their many applications, microjets have been widely employed to investigate water[8,9] and solute evaporation[7,10−12] and reactive gas uptake.[4,13−15]

Microjets can also be used to investigate gas−liquid chemical reactions by monitoring both the gas-phase reactant and gas-phase product. We explore the oxidation−reduction reaction, $N_2O_5(g) + 2Br^-(aq) \rightarrow Br_2(g) + NO_3^-(aq) + NO_2^-(aq)$, which is the bromide analogue of the ubiquitous chloride reaction, $N_2O_5(g) + Cl^-(aq) \rightarrow ClNO_2(g) + NO_3^-(aq)$.[16−21] Together, these aerosol-mediated reactions provide a means to transport reactive Br and Cl atoms into the troposphere following sunlight-driven photolysis of gaseous Br_2 or $ClNO_2$.[22] We pursue the bromide reaction here because of our ability to monitor Br_2 and inability to distinguish $ClNO_2$ and N_2O_5 using electron-impact ionization.[23−26] In addition to these halide reactions, N_2O_5 may also undergo hydrolysis to NO_3^- and H^+.[19,20] The branching to HNO_3, however, drops from 100% in pure water to less than 20% in 1 M NaCl.[27] In a reflection of the superior nucleophilicity of Br^- over Cl^- in protic solvents,[28,29] the branching from $ClNO_2$ to Br_2 exceeds 50% in a frozen salt mixture at just 1:30 NaBr/NaCl.[30]

Figure 1 illustrates a possible mechanism for Br^- attack on N_2O_5 in the near-interfacial region, leading initially to NO_3^- + $BrNO_2$.[16,17] The parallel reaction of Cl^- with N_2O_5 in water clusters has been investigated by electronic structure calculations[31] and by coupled ab initio molecular dynamics simulations and vibrational spectroscopy experiments.[32,33] On the basis of these studies, it is likely that Br^- attacks $NO_2^{\delta+}NO_3^{\delta-}$ during fluctuations that polarize the molecule,[34] forming short-lived $(BrNO_2NO_3)^-$ or directly ejecting NO_3^-

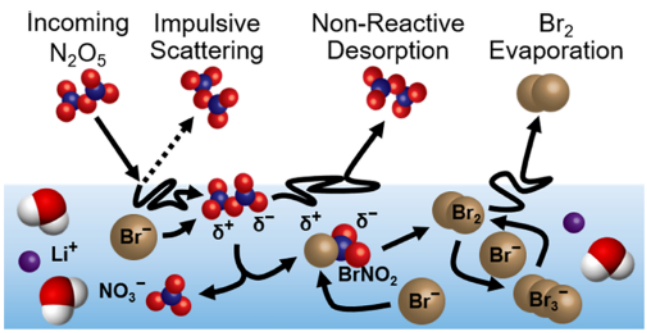

Figure 1. Possible pathways for collisions of N_2O_5 with a LiBr/H_2O solution and its oxidation of Br^- to Br_2. The species $BrNO_2$ and Br_3^- are likely reaction intermediates. N_2O_5 may also hydrolyze to $2NO_3^-$ + $2H^+$ (not shown).

Received: May 4, 2019
Revised: June 26, 2019
Published: June 28, 2019

DOI: 10.1021/acs.jpca.9b04225
J. Phys. Chem. A XXXX, XXX, XXX−XXX

in an S_N2 attack to form $BrNO_2$. Unlike $ClNO_2$ and Cl^-,[35,36] $BrNO_2$ reacts favorably with a second Br^- to produce Br_2 and NO_2^-,[16,37,38] with an equilibrium constant estimated to be 10^4 at 298 K (in comparison with an estimated equilibrium constant of 10^{-8} for Cl_2 formation).[39−41] The $BrNO_2$ intermediate has been identified in the gas phase in reactions of N_2O_5 with solid NaBr[42] and with dilute NaBr solutions.[17] Only Br_2 has been observed using concentrated bromide mixtures[30,38] and in field studies,[21] likely because $BrNO_2$ reacts before evaporating. As we emphasize later, Br_2 itself can react with a third Br^- to form the stable Br_3^- anion; this reversible complexation enhances the effective solubility of Br_2 and slows its evaporation.[43] These successive Br^- reactions are especially favorable in the 6 and 8 *m* (molal) LiBr solutions used in the present study, which correspond to 5 and 7 M LiBr and 1:9 and 1:7 LiBr/H_2O ratios, respectively. The highly soluble LiBr salt enables the solutions to be cooled to temperatures where the vapor pressure is a few Torr or lower in order to minimize collisions in the vapor cloud surrounding the microjet.[4,8] These temperatures were chosen to be 263 K for 6 *m* LiBr (2.1 Torr and 5 cP viscosity) and 240 K for 8 *m* LiBr (0.4 Torr and 13 cP).[44,45] Although LiBr itself is not found in sea spray, the high concentrations used here occur naturally in aged aerosol particles. In particular, the NaCl concentration jumps from 0.5 *m* in the ocean to 6 *m* in aerosol particles as the relative humidity drops to 76% and water evaporates from the particles.[46−48]

We use gas-microjet scattering experiments to explore reactions of N_2O_5 with pure LiBr/H_2O solutions and then learn how its reactivity is altered by the addition of a nonionic surfactant, 1-butanol, and a cationic surfactant, tetrabutylammonium bromide (TBABr). These experiments enable us to monitor the outcome of a gas-microjet reaction from the gas-phase reactant to gas-phase product by tailoring the interfacial region of an aqueous solution.

■ EXPERIMENTAL PROCEDURE

The scattering apparatus in Figure 2 depicts the LiBr/H_2O reservoir, microjet assembly, N_2O_5 beam, and mass spectrometer detector. Each component is discussed below.

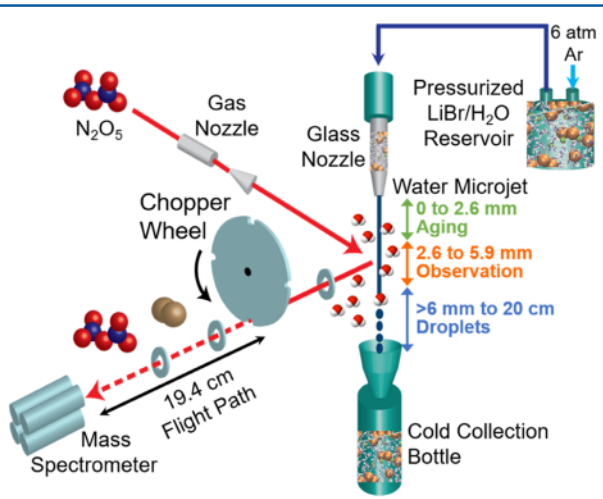

Figure 2. Microjet scattering apparatus for exploring collisions of N_2O_5 with a 35 μm diameter jet moving at 30 m s^{-1}. The aging, observation, and droplet distances are indicated along the jet.

Microjet Generation. Solutions of 6.0 ± 0.1 and 8.0 ± 0.1 *m* LiBr are prepared by dissolving the salt (99% Alfa Aesar) in Millipore water, filtering to remove insoluble residues, and suctioning the surface of the solution to remove insoluble surfactants inadvertently introduced by the salts or water. Surfactant mixtures of TBABr (≥98% Sigma-Aldrich) and 1-butanol (99.8% Sigma-Aldrich) are made by mixing them into the LiBr solutions. The 6 and 8 *m* solutions are then pressurized with Ar gas to ∼6 and ∼2 atm, respectively, and forced through a tapered glass nozzle with an outer diameter of 6.4 mm and an inner exit diameter of 35 μm, as determined from microscopic images. A variably cooled copper block just above the glass nozzle lowers the temperatures of the 6 and 8 *m* solutions to 270 and 258 K, respectively. The 6 *m* LiBr jet travels at speeds of 30−32 m s^{-1} and evaporatively cools to an average temperature of 263 ± 15 K within an observation region located 2.6−5.9 mm from the nozzle exit, as depicted in Figure 2. Similarly, the 8 *m* LiBr jet travels at a slower speed of 17 m s^{-1} and evaporatively cools to 240 ± 10 K. These jet temperatures are predicted to within the error bars by evaporative cooling calculations in refs.[1,4] Jet breakup then leads to droplet formation at ∼7 mm (6 *m* LiBr) and ∼6 mm (8 *m* LiBr) from the nozzle.[1] These droplets pass through the chamber and are collected in a vacuum flask cooled to 200 K. The interaction region is surrounded by liquid nitrogen-cooled panels, which, along with a baffled 2300 L s^{-1} diffusion pump, capture water and N_2O_5 molecules and maintain the pressure below 1×10^{-5} Torr.

N_2O_5 Incident Beam. Low translational energy (10 kJ mol^{-1}) N_2O_5 molecules are generated to measure N_2O_5 uptake into solution at near-thermal collision energies, whereas high translational energy (∼100 kJ mol^{-1}) N_2O_5 molecules are used to monitor Br_2 production. This high-energy N_2O_5 beam is employed to detect the weak Br_2 signal because its greater speed generates an incoming flux that is ∼40 times larger than the 10 kJ mol^{-1} beam (the flux of the 100 kJ mol^{-1} beam is estimated to be 10^{17} cm^{-2} s^{-1}, which delivers 10^{-2} monolayers of N_2O_5 to the surface over the 110 μs exposure time).

N_2O_5 is synthesized by oxidizing NO gas with O_3 and trapping the product in a glass vessel submerged in a dry ice-ethanol bath.[49] A beam of 10 kJ mol^{-1} N_2O_5 is created from its vapor at 261 K (20 Torr vapor pressure) as it expands supersonically from a 100 μm diameter pinhole nozzle heated to 353 K to minimize cluster formation. The 100 kJ mol^{-1} N_2O_5 beam is generated by passing H_2 over the N_2O_5 sample at 261 K and expanding the 700 Torr mixture through the same nozzle. Before entering the gas nozzle, the N_2O_5 gas is purified in two steps to remove HNO_3 arising from the hydrolysis of N_2O_5 with residual water: the gas stream first passes through a P_2O_5 glass-bead trap to oxidize HNO_3 back into N_2O_5 and then passes through a trap filled with nylon mesh that irreversibly reacts with HNO_3. As shown later, the N_2O_5 beam still contains on average 11% HNO_3. The heated nozzle may also decompose a fraction of N_2O_5 into NO_2 and NO_3, predicted by equilibrium calculations to be just 0.3% at 353 K and 20 Torr.[50] A search for NO_3 at its parent ion mass of 62 Da (∼15% ionization branching fraction[51] and ∼60% ionization probability relative to N_2O_5[52]) yielded a similar 0.3 ± 0.3% NO_3 fraction.

Detection of Gas-Phase Species. Unreacted N_2O_5 molecules scattering and desorbing from the microjet, along with the evaporating Br_2 product, are detected at 90° from the incident beam by a doubly differentially pumped mass

DOI: 10.1021/acs.jpca.9b04225
J. Phys. Chem. A XXXX, XXX, XXX−XXX

spectrometer equipped with electron impact ionization. Molecules traveling toward the detector are chopped into 57 μs pulses by a spinning slotted wheel, as shown in Figure 2, and their arrival times over a 19.4 cm flight path are recorded as a time-of-flight (TOF) spectrum. A vertical slit aperture positioned in front of the chopper wheel limits the viewing region of the detector to a 3.3 mm segment of the jet, from 2.6 to 5.9 mm below the nozzle tip, in order to minimize background signals and reduce the observed temperature gradient along the microjet. This aperture and two additional ones pictured in Figure 2 prevent molecules scattering off the tip of the glass nozzle from entering the mass spectrometer. The glass nozzle may also be intentionally placed in the scattering region by translating the nozzle downward and moving it slightly away from the mass spectrometer to intersect a larger glass area.

Microjet Temperature. Average jet temperatures in the 2.6−5.9 mm observation region are determined by monitoring the speed distribution of evaporating argon atoms dissolved in solution.[4] To generate an argon-saturated solution, the liquid reservoir is evacuated, filled with Ar gas, and then physically shaken to mix the gas and liquid. Figure 3a shows that Ar atoms desorb from the jet in an approximate Maxwell−Boltzmann (MB) distribution that is fit to a temperature of 263 K, along with fits at ±15 K. None of the MB fits are exact because the Ar atoms expand slightly supersonically through the vapor cloud, implying that some evaporating Ar and H_2O collide as they exit the jet.[8,10,53,54] Figure 3b illustrates that water molecules themselves evaporate in a more developed supersonic expansion because of the larger cross section for water−water collisions in the jet vapor cloud.[7] This distribution is more Maxwellian at 240 K than at 263 K because of the drop in water vapor pressure from 2.1 to 0.4 Torr. Smaller jet diameters also lead to more Maxwellian distributions but reduce the scattering signals proportionately.[10,12]

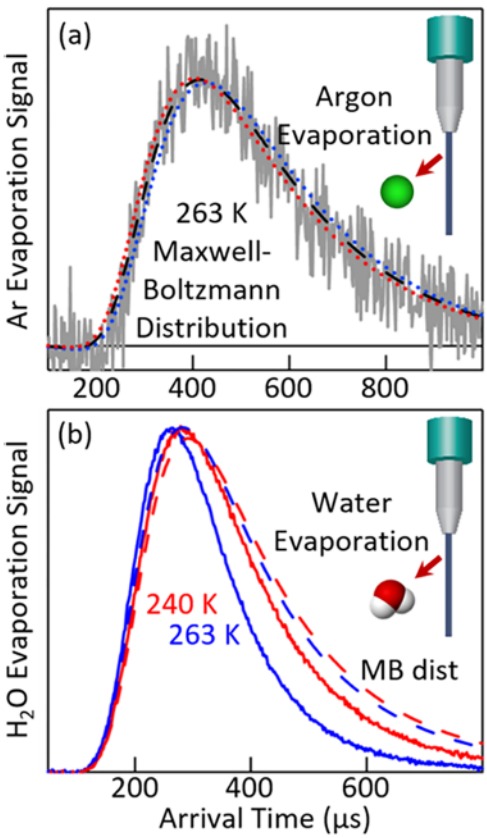

Figure 3. TOF spectra of evaporating (a) argon atoms and (b) water molecules from a 6 *m* LiBr/H_2O jet. In (a), the black dashed line is a best fit to a MB distribution at 263 K, along with dotted MB fits at ±15 K. In (b), the observed H_2O TOF spectra are compared to temperatures at 240 and 263 K determined by Ar evaporation: the faster and narrower water spectra reflect H_2O−H_2O collisions in the vapor cloud surrounding the jet.

Surface Tension Measurements. The surface tensions of the salt and surfactant solutions are measured by the Wilhelmy plate method. Measurements are performed at each concentration by monitoring the force acting on a 16.5 mm × 0.1 mm Pt plate within a N_2-purged enclosure. The deviations between independent runs are found to be roughly ±0.5 mN m^{-1}.

■ RESULTS AND DISCUSSION

We carried out five distinct experiments to investigate reactions of N_2O_5 with 8 and 6 *m* LiBr solutions at 240 and 263 K: (1) measurements of N_2O_5 reactive uptake, (2) observation of the Br_2 reaction product, (3) benchtop surface tension and surface composition measurements of TBABr and butanol solutions, (4) estimates of the microjet surface composition by high-energy SF_6 scattering, and (5) investigations into surfactant control of Br_2 production and evaporation.

Measurement of N_2O_5 Uptake. We first attempted to measure the irreversible, reactive uptake of N_2O_5 into 8 *m* LiBr/H_2O at 240 K using the beam reflectivity method.[55] Details are provided in ref 15, where we successfully used this approach to determine the entry probability of organic acids and bases into LiBr/H_2O microjets. Briefly, the flux of N_2O_5 molecules that impinge on the jet surface is compared with the flux of molecules that do not react and instead return to the gas phase. This outgoing N_2O_5 flux is monitored by recording the TOF spectrum of N_2O_5 (at NO_2^+) desorbing from the jet when it is exposed to the gas. The incoming N_2O_5 flux is not measured directly but is instead monitored by recording the TOF spectrum when the incident N_2O_5 beam reflects from the nonreactive borosilicate glass nozzle. Because the 6.4 mm diameter glass nozzle and 35 μm diameter water microjet have such different sizes, we calibrate the N_2O_5 scattering signal by comparing it with the scattering of argon, a perfectly nonreactive gas. The fraction of escaping N_2O_5 molecules is then calculated from $P_{escape} = (J/G)_{NO_2}/(J/G)_{Ar}$, where J is the gas flux from the microjet and G is the gas flux from the glass nozzle.[15] P_{escape} can vary from 0, where all N_2O_5 molecules react with the jet and do not escape, to a value of 1, where no N_2O_5 molecules react and instead behave like Ar atoms. The reactive uptake probability P_{uptake} (also called the uptake coefficient γ) is then equal to $1 - P_{escape}$. We use low translational energy, 10 kJ mol^{-1} (5 RT_{liq}) N_2O_5 molecules in order to ensure that nearly all impinging N_2O_5 molecules thermally equilibrate at the surface upon collision, a likely prerequisite for the reaction (as discussed later).[56−60]

Figure 4 illustrates how Ar atoms and N_2O_5 molecules interact with the 8 *m* LiBr/H_2O jet and glass nozzle. Panel a shows the TOF spectrum of Ar atoms scattering from the glass nozzle at a near-thermal collision energy of E_{inc} = 7 kJ mol^{-1}. The small signal near the baseline is the TOF spectrum of Ar

DOI: 10.1021/acs.jpca.9b04225
J. Phys. Chem. A XXXX, XXX, XXX−XXX

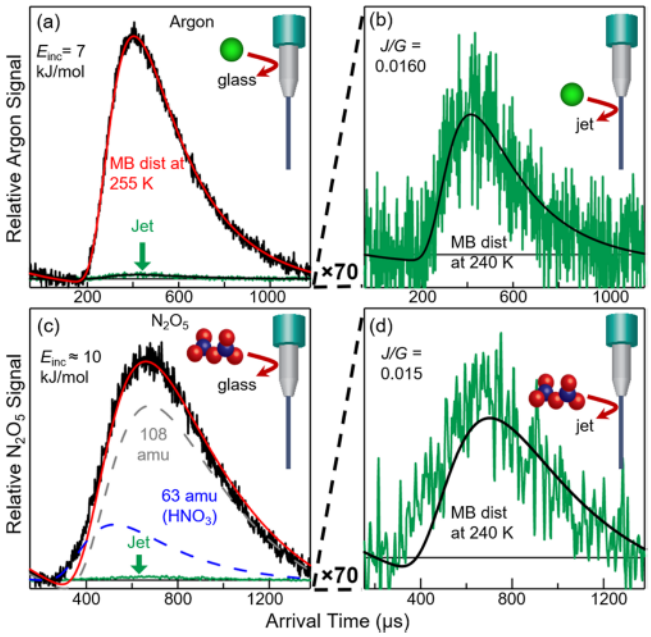

Figure 4. TOF spectra of argon atoms following collisions with the (a) glass nozzle and (b) 8 *m* LiBr/H_2O jet, along with TOF spectra of N_2O_5 molecules following collisions with the (c) glass nozzle and (d) jet. The weak jet spectra are also shown in (a,c) and are enlarged by 70-fold in (b,d). *J*/*G* refers to the ratio of the fluxes of Ar or N_2O_5 desorbing from the jet (*J*) and glass nozzle (*G*).

scattering from the 170-fold smaller microjet surface. This jet spectrum is enlarged by a factor of 70 in Figure 4b. MB fits to the TOF spectra reveal temperatures of 258 K for the glass nozzle and 240 K for the jet, which has further cooled by evaporation. The value of *J*/*G* for Ar is 0.0160 ± 0.0009 (90% confidence interval for 11 independent measurements). This value is larger than the geometric jet-to-glass nozzle diameter ratio of 0.0055 because the mass spectrometer does not view the entire width of the glass nozzle and because the actual size of the microjet is slightly larger than the exit diameter of the nozzle.[1]

Panels c and d of Figure 4 show TOF spectra for N_2O_5 molecules scattering from the 8 *m* LiBr/H_2O solution and the glass nozzle. The tiny signal near the baseline in panel c is the TOF spectrum for N_2O_5 desorbing from the microjet, which is enlarged in panel d. The imperfect fit to a 240 K MB distribution is likely caused by collisions between desorbing N_2O_5 and H_2O molecules in the vapor cloud surrounding the microjet. We tested this idea by scattering $CHCl_3$ from the jet and glass nozzle. This nonreactive molecule was chosen because it is similar in mass and size to N_2O_5 and is weakly soluble.[41] While the $CHCl_3$ nozzle spectrum fits an MB distribution at 255 K, just like Ar, the $CHCl_3$ jet spectrum is similar in shape to the N_2O_5 jet spectrum in panel d (see the Supporting Information for comparison of $CHCl_3$ and N_2O_5 spectra).

An additional complicating feature in measuring N_2O_5 uptake is the presence of HNO_3 impurity in the N_2O_5 incident beam, as both molecules ionize primarily to NO_2^+ (m/z = 46) in the mass spectrometer.[24−26] These impinging HNO_3 molecules are expected to enter and dissolve into the 240 K solution on every collision and remain for long times.[56,61−64] Thus, even a small fraction of HNO_3 in the incident beam will interfere with the N_2O_5 uptake measurement. We attempted to correct for the presence of HNO_3 by decomposing the N_2O_5 TOF spectrum from the glass nozzle in panel c into two Maxwellian components: one for HNO_3 (63 Da) and another for N_2O_5 (108 Da). This decomposition assigns a fraction f = 84% of the spectrum in panel c to N_2O_5 and the remaining 16% to HNO_3, both detected at NO_2^+. Independently, we determined the relative ionization probabilities β of N_2O_5 and HNO_3 to NO_2^+ (m/z = 63) in the electron impact ionizer to be $NO_2^+(N_2O_5)/NO_2^+(HNO_3)$ = 0.65.[23] The true fraction h of N_2O_5 in the incident beam is then $h = f/[f + (1 - f)\beta]$ = 90%. The NO_2^+ signal arising from N_2O_5 is equal to $h \cdot G_{NO_2}$, and P_{uptake} equals $1 - (J/hG)_{NO_2}/(J/G)_{Ar}$. Averaged over all measurements, we found h to be 0.89 ± 0.04.

The N_2O_5 uptake measurements in Figure 4 were repeated 11 times, yielding an average reactive uptake probability of −0.05 ± 0.10 (90% confidence interval). Negative values cannot be real, but the large confidence interval encompasses small positive values as well. This broad distribution reflects the challenges of measuring small uptake probabilities using high vapor pressure microjets in the presence of a highly reactive impurity. In comparison, N_2O_5 uptake into saturated NaCl solutions is measured to be close to 0.03 at 298 K and rises to 0.19 when in contact with 23 *m* sulfuric acid at 240 K, the highest value recorded.[18,20,22,65] We estimate that this 0.19 reaction probability value would have caused a 23% reduction in our measured jet spectrum and should have been discernible, implying that reactive loss of N_2O_5 to 8 *m* LiBr/H_2O at 240 K very likely occurs with a probability lower than the current 0.19 maximum.

One inference from the small inferred uptake is that the greater nucleophilicity of Br^- over Cl^- does not substantially lead to enhanced capture of N_2O_5 molecules, at least not beyond the previous 0.03−0.19 measurements quoted above. Perinne et al. have shown that Br^- and Li^+ are both surface-active ions in water, each having oscillatory depth profiles.[5] In particular, the Br^- ion concentration within the outermost water layer of a 2 M LiBr solution is very close to its bulk phase value and the Li^+ ion concentration peaks just below this layer. If the Br^- interfacial concentration in our 8 *m* (7 M) LiBr solution is also equal to the bulk concentration, then these Br^- ions are on average spaced 6 Å apart. The N_2O_5 entry probability has been measured by Gržinić et al.[66] to be greater than 0.4 at 298 K and perhaps approaches 1 at 240 K. In this case, nearly all N_2O_5 molecules interact within an interfacial region in which they are typically separated by one water molecule (3 Å) from a Br^- ion, likely making contact several times with these ions before desorbing into the gas phase. The actual contact time and penetration depth of N_2O_5 molecules into the 240 K LiBr solution are not known; simulations by Hirschberg et al. indicate that the adsorption time exceeds 25 ps on the surface of pure water at 298 K.[34] This interaction time should be longer at 240 K, but based on our measurements, it is still too short to allow N_2O_5 to react with Br^- on most collisions.

Production of Gaseous Br_2. In contrast to our difficulties in measuring N_2O_5 uptake using low-energy N_2O_5 molecules, we were able to measure the Br_2 product using 100 kJ mol^{-1} N_2O_5 molecules, whose high speed provides 40 times the flux of the low-energy beam. We have used these high-flux beams in previous studies of collisions of HCl with sulfuric acid,[56] DCl with pure glycerol,[67] and Cl_2 and N_2O_5 with glycerol

DOI: 10.1021/acs.jpca.9b04225
J. Phys. Chem. A XXXX, XXX, XXX−XXX

containing NaBr and surfactants.[38,68] In each case, the trapping probability decreases with increasing collision energy, but the fraction of impinging molecules that react scales with the fraction that fully dissipate their excess energy and become trapped (adsorbed). This scaling implies that trapping precedes reaction with solute or solvent species. For 100 kJ mol^{-1} collisions of N_2O_5 with 8 *m* LiBr/H_2O at 240 K, Figure 5 reveals that energy dissipation into surface and subsurface

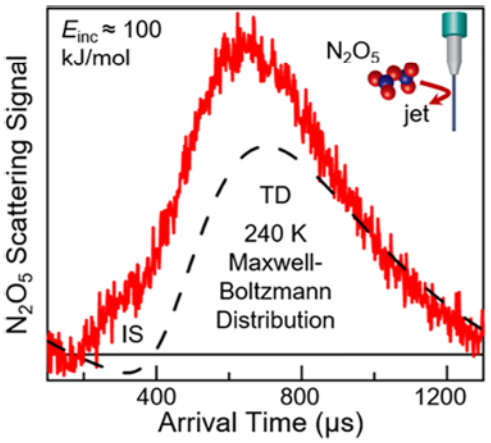

Figure 5. TOF spectrum of nonreactive N_2O_5 undergoing TD and IS following collisions of 100 kJ mol^{-1} N_2O_5 with 8 *m* LiBr at 240 K. The large TD signal (corresponding to 65% of the outgoing flux) implies extensive energy dissipation and thermal equilibration of high-energy N_2O_5 molecules at the surface of the microjet.

H_2O must be rapid in order for the N_2O_5 thermal desorption (TD) signal to be so strong.[34] Parallel behavior is observed for collisions of N_2O_5 with the surface of ice, where thermalization is also extensive.[59] Recent experiments by Langlois et al. further suggest that impinging N_2O_5 molecules that do not thermalize at the surface of water almost always scatter back into the gas phase: the probability for direct embedding of a molecule at 100 kJ mol^{-1} with the mass of N_2O_5 below the interfacial region of amorphous ice is only 0.1%.[69] On the basis of these studies, we were motivated to use a high-energy and high-flux beam to observe reactions of N_2O_5 adsorbed on the surface of the LiBr/H_2O microjet.

Figure 6a demonstrates that N_2O_5 can indeed react with Br^- in a 6 *m* LiBr jet at 263 K to produce product Br_2. These Br_2 molecules do not evaporate in a Maxwellian distribution, most likely because of collisions between Br_2 and outgoing H_2O molecules in the vapor cloud surrounding the jet at 263 K (P_{vap} = 2.1 Torr), which in turn generate a moderately supersonic expansion. The approach to a Maxwellian distribution can be seen in panel b, which displays Br_2 evaporating from an 8 *m* LiBr jet at 240 K (P_{vap} = 0.28 Torr), as determined by Ar evaporation. This lower vapor pressure jet spectrum is better fit by a 240 K MB distribution but is still slightly supersonic (in accord with the non-Maxwellian N_2O_5 jet spectrum in Figure 4d).

As illustrated in Figure 1, the Br_2 product that is created by the sequential attack of Br^- on N_2O_5 can react reversibly with a third Br^- to generate Br_3^-, especially in concentrated Br^- solutions. The physical solubility H_{phys} of Br_2 is close to 4 M atm^{-1} in supercooled water at 263 K, a low value that would lead to rapid evaporation for Br_2 produced near the surface.[70] The solubility of Br_2, however, is greatly enhanced by Br_3^- formation, whose favorable equilibrium is estimated to be K_{eq}

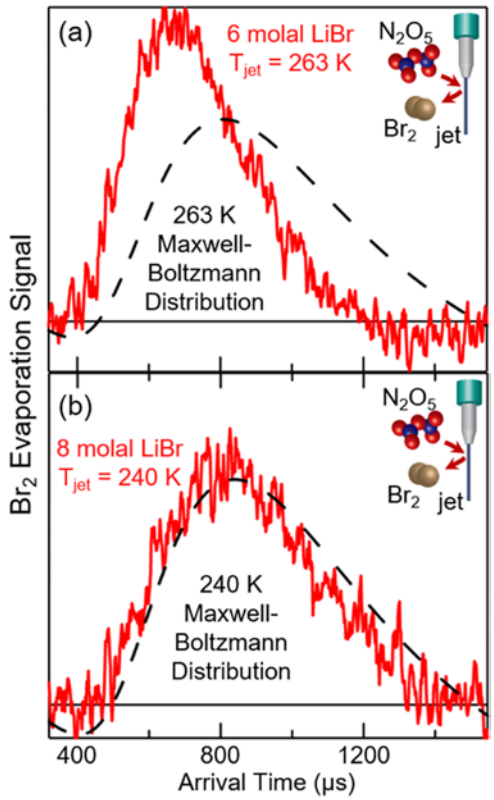

Figure 6. TOF spectra of evaporating product Br_2 following reaction between N_2O_5 and Br^- in (a) 6 *m* LiBr at 263 K and in (b) 8 *m* LiBr at 240 K. The black dashed lines are MB distributions at 263 K in (a) and 240 K in (b). The solution temperatures, T_{jet}, are determined by Ar evaporation.

= 16 for $Br^- + Br_2 \rightleftharpoons Br_3^-$ in 6 *m* (5 M) LiBr at 263 K.[43] This reaction leads to an effective solubility $H_{eff} = H_{phys}(1 + K_{eq}[Br^-])$ = 360 M atm^{-1}, which causes Br_2 to evaporate at a slower rate. We estimate in the Appendix that the characteristic residence time τ of Br_2 in solution increases from much less than 1 to ~6 μs because of Br_3^- formation, a time that corresponds to diffusion over a depth $z \approx (D\tau)^{1/2}$ = 400 Å for $D = 2.4 \times 10^{-6}$ cm^2 s^{-1}.[71] In this case, roughly 90% of the Br_2 molecules evaporate during the 110 μs observation time of the jet.

The identification of Br_2 enables us to learn which parameters control its production in the near-interfacial region, including solution temperature, LiBr concentration, effects of dissolved NO_3^- and NO_2^- on intermediate steps, and the presence of nonionic, ionic, and reactive surfactants. We chose in this study to investigate two surfactants, a nonionic alcohol that may block entry and alter interfacial Br^- concentrations and a cationic surfactant that complexes with the Br_3^- intermediate. The surface behavior of these surfactants and their ability to alter N_2O_5 reactivity and Br_2 release into the gas phase are described below.

Characterizing Surfactant Concentrations at the Microjet Surface. We find that the Br_2 signal in Figure 6 can be controlled by the addition of the nonionic surfactant 1-butanol and the cationic surfactant TBA^+/Br^-. To make these observations quantitative, we first made measurements of their equilibrium surface concentration in 6 *m* LiBr solutions at 298 K and then used SF_6 scattering to gauge their surface concentrations in the microjet itself.

DOI: 10.1021/acs.jpca.9b04225
J. Phys. Chem. A XXXX, XXX, XXX−XXX

Surface Concentrations of TBABr and 1-Butanol. The surface concentrations c_{surf} were calculated from the Gibbs adsorption equation, $c_{surf} \approx (-1/RT)(\partial\gamma/\partial \ln c_{bulk})_T$, assuming unit activity coefficients for the bulk surfactant concentration c_{bulk}.[72] Figure 7 displays the surface tensions and surface concentrations of TBA^+ and 1-butanol, along with fits to the two-parameter Langmuir adsorption isotherm, $c_{surf} = c_{inf}(Kc_{bulk}/(1 + Kc_{bulk}))$. The TBA^+ surface concentration rapidly saturates at 1.1×10^{14} cm^{-2}. This corresponds to roughly 58% of a compact monolayer assuming a tight packing area of 54 $Å^2$ for TBA^+ estimated from ref 73. In contrast, the 1-butanol concentration rises more slowly and reaches 2.2×10^{14} cm^{-2} at the 0.020 *m* concentration used here, equal to ~44% of a compact all-trans monolayer assuming a close-packed area of 20 $Å^2$.[74] Simulations of the loosely packed tetrabutylammonium iodide (TBAI)/H_2O and 1-butanol/5 M NaI/H_2O surfaces at similar concentrations are shown later in Figures 8a and 10a.[32,75,76]

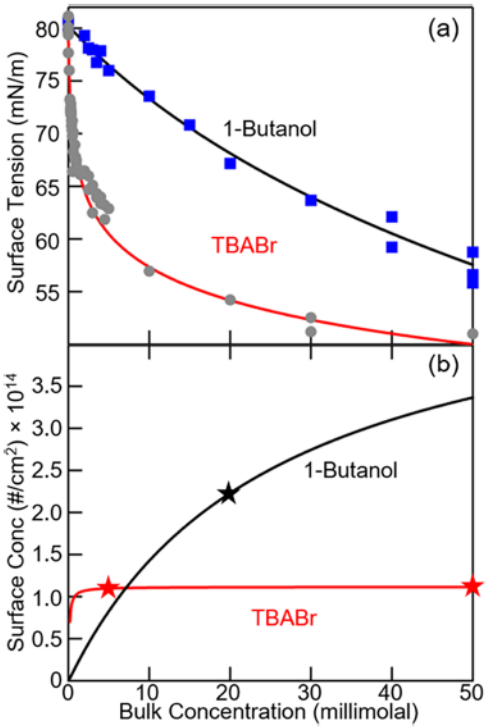

Figure 7. (a) Benchtop surface tension measurements of 6 *m* LiBr solutions at 298 K upon addition of 1-butanol, blue squares, and TBABr, gray circles. (b) Surface concentrations of 1-butanol and TBABr obtained from (a) using the Gibbs–Langmuir equation $\gamma(\text{pure}) - \gamma(c_{bulk}) = c_{inf}RT \ln(1 + Kc_{bulk})$. The parameters are c_{inf}(1-butanol) = 5.1×10^{14} cm^{-2} and c_{inf}(TBABr) = 1.1×10^{14} cm^{-2} and K(1-butanol) = 39 m^{-1} and K(TBABr) = 1.7×10^4 m^{-1}. The stars represent concentrations used in the experiments.

High-Energy SF_6 Scattering to Probe Surfactant Surface Composition. The fast ~30 m s^{-1} speed of the microjet limits the time for 1-butanol and TBA^+ to diffuse to the surface when the jet reaches the middle of the observation region in ~140 μs. This short time may be insufficient for full segregation to the equilibrium values in Figure 7. To estimate the concentration of the surfactant in the observation region itself, we use high-energy SF_6 scattering to detect the presence of hydrocarbon chains and Br^- ions at the microjet surface. We have used this technique before with argon scattering to detect surfactants at the surface of sulfuric acid and glycerol,[38,75] but we found that high-energy 90 kJ mol^{-1} Ar collisions are not sensitive enough for aqueous salt solutions. The more massive SF_6 molecule can be accelerated to higher energies of 300 kJ mol^{-1} and generates more discernible patterns in the TOF spectrum. As pictured in Figure 8a,[75] impinging SF_6 molecules may impulsively scatter (IS channel, short arrival times corresponding to high velocities) from the $TBA^+/Li^+/Br^-/H_2O$ surface in one or a few collisions, measured in panel b to retain on average 1/10 of their translational energy. The remaining SF_6 molecules fully dissipate their excess energy and

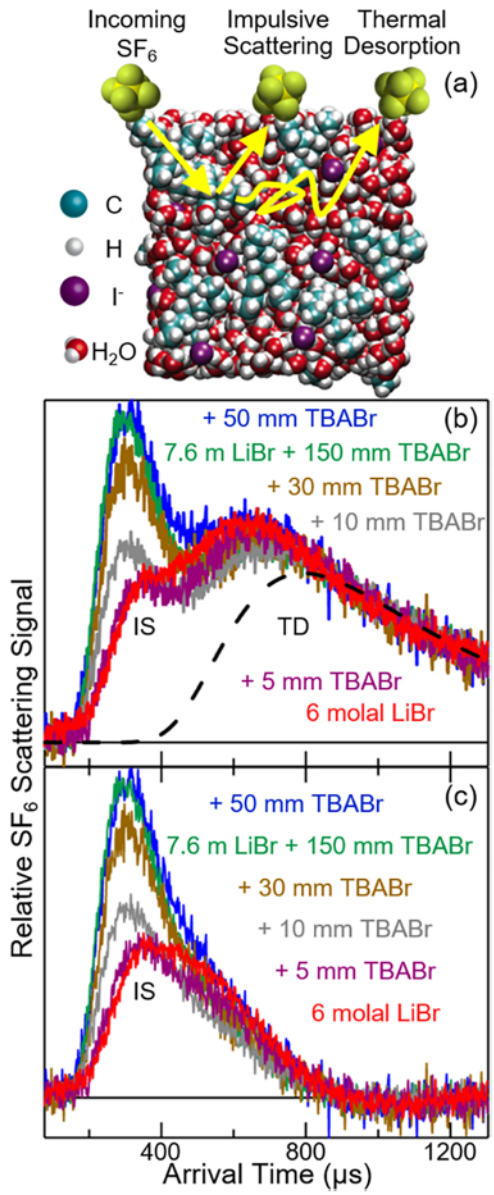

Figure 8. (a) Scattering diagram of SF_6 impinging on a surface containing TBAI. The molecular dynamics simulation is a top view of TBAI on water at a surface concentration of 0.9×10^{14} cm^{-2}, reprinted from ref 75. (b) TOF spectra of SF_6 following collisions of high-energy SF_6 with 6 *m* LiBr at 263 K containing 0, 5, 10, 30, and 50 m*m* TBABr and 7.6 *m* LiBr containing 150 m*m* (millimolal) TBABr. The black dashed line is a MB fit at 263 K corresponding to SF_6 TD. (c) IS component from each spectrum in (b). This IS component is obtained by subtracting the TD component from each TOF spectrum. Each spectrum is displayed after normalizing by the magnitude of its TD flux.

DOI: 10.1021/acs.jpca.9b04225
J. Phys. Chem. A XXXX, XXX, XXX−XXX

then thermally desorb (TD channel, long arrival times and low velocities), propelled into vacuum by thermal motions of the surface species. Figure 8b shows SF_6 scattering from 6 *m* LiBr at 263 K mixed with 0, 0.005, 0.010, 0.030, and 0.050 *m* TBABr and 7.6 *m* LiBr mixed with 0.1500 *m* TBABr. As the TBABr concentration is increased, the direct scattering component also increases, accompanied by a small decrease in TD. We tentatively attribute this growth in direct scattering to collisions of SF_6 with individual surface TBA^+ ions, either surrounded by H_2O or bound tightly to Br^-. These species are substantially more massive than H_2O itself, and so their segregation to the surface may cause impinging SF_6 molecules to lose less energy upon impact.[77] Figure 8c isolates just this direct scattering component, which reaches a steady signal strength near c_{bulk} = 0.050 *m* TBABr. As in previous studies utilizing high-energy Ar scattering, we correlate changes in the ratio *r* of IS to TD fluxes with changes in TBABr surface composition c_{surf}. This map is shown in Figure 9, constructed from the relation[78]

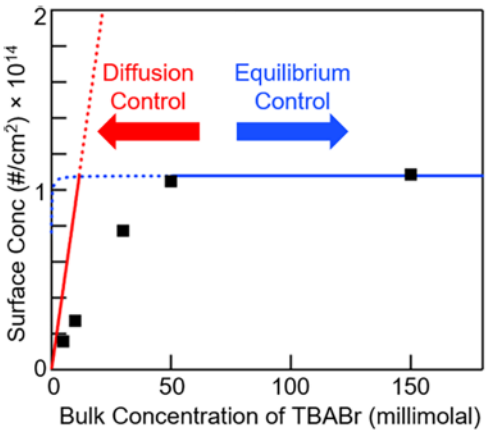

Figure 9. TBABr surface concentration determined by SF_6 scattering in the observation region of the microjet (black squares). The *y*-axis is calculated from the relative sizes of the IS components in Figure 8b according to eq 1. The red line is the zero-coverage prediction, given by $c_{surf} = (4Dt/\pi)^{1/2}c_{bulk}$. The blue line is the equilibrium surface concentration obtained in Figure 7.

$$c_{surf}(c_{bulk})/c_{surf}(0.05\ m\ \text{TBABr}) = (\text{change in observed IS/TD ratio due to surfactant})/(\text{maximum monolayer change}) = [r(c_{bulk}) - r(\text{pure LiBr})]/[r(0.05\ m\ \text{TBABr}) - r(\text{pure LiBr})] \quad (1)$$

Figure 9 implies that the TBA^+/Br^- surface concentration steadily increases until approximately 0.050 *m*. The red line corresponds to the prediction for filling an empty surface, where every TBA^+ that diffuses to the surface sticks to it. In this diffusion-controlled case, $c_{surf} = (4Dt/\pi)^{1/2}c_{bulk}$,[79] plotted using $D = 1.2 \times 10^{-6}$ cm^2 s^{-1} and t = 140 μs.[80] The measurements increasingly deviate from this line as the empty surface sites fill up with TBA^+.

The neutral surfactant 1-butanol behaves differently from TBA^+/Br^-, as shown in Figure 10. The addition of 0.02 *m* butanol to 6 *m* LiBr suppresses the direct scattering of SF_6, perhaps because the individual butyl chains are more flexible than the tethered chains in TBA^+ and because the neutral molecule is not paired with Br^-. This surfactant is predicted to diffuse slightly faster than TBA^+, and according to Figure 9 and $D = 1.8 \times 10^{-6}$ cm^2 s^{-1},[81] it likely reaches a surface concentration close to 2.0×10^{14} cm^{-2}, just below its equilibrium value of 2.2×10^{14} cm^{-2}. This microjet surface concentration corresponds to 40% of a compact monolayer.

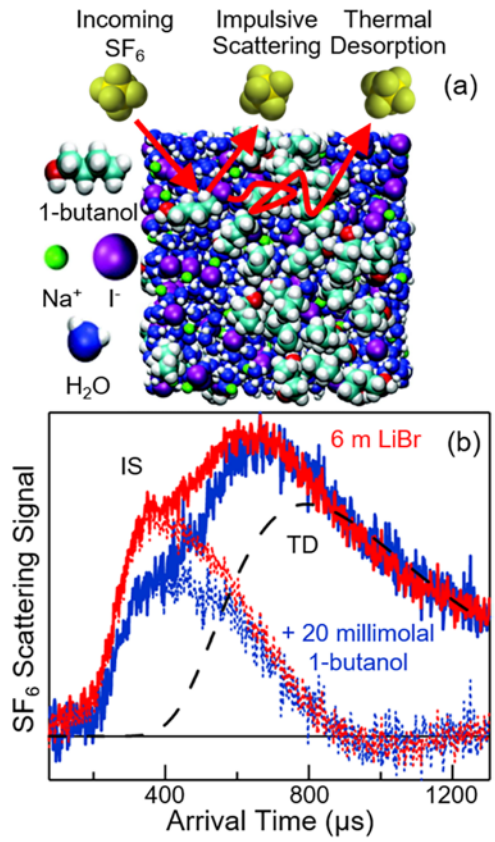

Figure 10. (a) Pathways for collisions of SF_6 with a $LiBr/H_2O$ solution with 1-butanol molecules at the interface. The molecular dynamics simulation shows the top view of 1-butanol on a 5.0 M NaI/H_2O solution at a surface concentration of 2.8×10^{14} cm^{-2}, reprinted from ref 76. (b) TOF spectra of SF_6 following collisions of high-energy SF_6 with 6 *m* LiBr at 263 K containing 0 and 20 m*m* 1-butanol. The black dashed line is a MB distribution at 263 K corresponding to SF_6 TD. The red and blue dotted curves are the IS components, obtained by subtracting the TD component from each spectrum.

Effects of 1-Butanol and TBA^+/Br^- on Br_2 Production and Evaporation. We anticipated that partial monolayers of butanol would hinder N_2O_5 entry into the Br^--rich interfacial region based on previous observations that a hexanoic acid monolayer on artificial seawater and butanol and hexanol monolayers on sulfuric acid each reduce N_2O_5 hydrolysis.[82,83] Figure 11 compares Br_2 production from bare 6 *m* LiBr at 263 K and the 0.02 *m* butanol solution analyzed above. The spectra indicate that the butanol monolayer, at 40% of a compact monolayer, suppresses the Br_2 signal to 0.65 of its value from pure LiBr. This reduction is remarkably similar to our previous measurement of N_2O_5 uptake into a 44% coverage butanol monolayer on 72 wt % H_2SO_4 at 216 K, which revealed that butanol suppresses N_2O_5 uptake to 0.65 ± 0.16 of its value on the pure acid solution.[83] We do not yet know if this suppression arises because the butyl chains restrict contact of

DOI: 10.1021/acs.jpca.9b04225
J. Phys. Chem. A XXXX, XXX, XXX−XXX

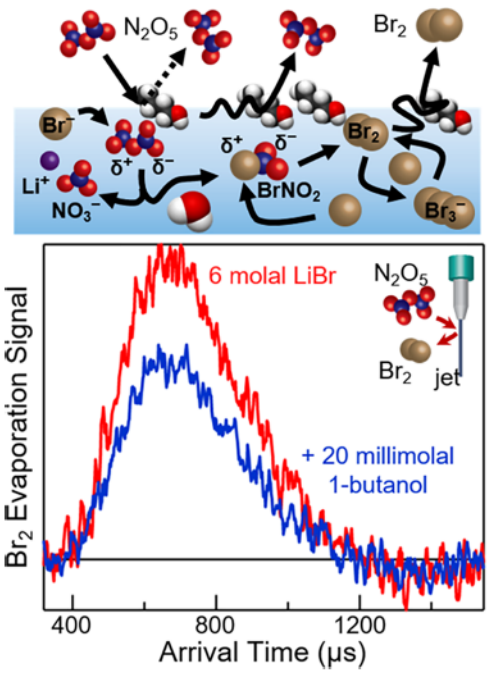

Figure 11. TOF spectra of product Br_2 evaporating from 6 *m* LiBr (red) and with 20 m*m* 1-butanol added to solution (blue). The Br_2 signal is reduced by 35% upon addition of 1-butanol.

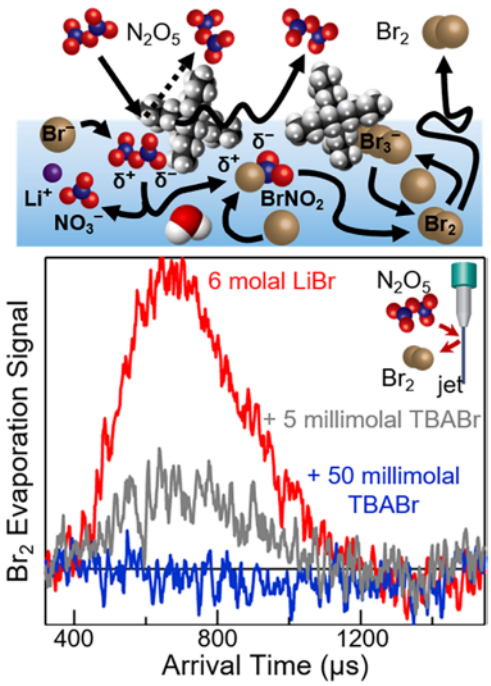

Figure 12. TOF spectra of product Br_2 evaporating from 6 *m* LiBr (red) and with 5 m*m* (gray) and 50 m*m* (blue) TBABr added to solution. The Br_2 signal is reduced by 85% upon addition of 5 m*m* TBABr and is not detected upon addition of 50 m*m* TBABr.

the N_2O_5 molecules with interfacial ions or if the monolayer itself alters the Br^- and Li^+ concentrations near the butanol OH group. This second explanation is inspired by the studies of Krisch et al., who found that the high interfacial I^-/K^+ ratio in a saturated KI solution at 263 K decreases toward one when butanol is spread on the surface and both K^+ and I^- interact with the buried butanol OH group.[76] An analogous interfacial reduction in Br^- and an increase in Na^+ were measured by Lee et al. when citric acid was added to dilute NaBr solutions.[14,84] Within this picture, the 35% Br_2 suppression we observe may be partly caused by an interfacial reduction in Br^- ions or preferential interaction of Br^- with butanol if N_2O_5 samples just the top layers of the solution before desorbing back into the gas phase.

The effects of TBABr are even more striking. Figure 12 shows that the addition of 0.005 *m* TBABr reduces the Br_2 evaporation signal to 15% of its pure value and the addition of 0.050 *m* TBABr eliminates the Br_2 signal. The surface concentrations in these cases are 1.6×10^{13} cm^{-2} (9% of a compact monolayer) and 1.1×10^{14} cm^{-2} (58% of a compact monolayer). In comparison to the reduction to 65% of the pure value by the butanol monolayer, the sharp reductions caused by TBABr suggest that physical blocking by the butyl chains may not be the sole explanation for the reduced Br_2 signal. Our earlier studies of tetrahexylammonium bromide (THABr) in glycerol indicate that this cationic surfactant actually enhances Br_2 production by drawing more Br^- ions to the surface.[38] These studies were carried out using a slowly rotating coated wheel that can monitor reaction times up to several seconds; they showed that the addition of 0.03 M THABr to a 2.7 M NaBr/glycerol solution extends the lifetime of Br_2 from 30 μs to greater than 0.1 s, which we attributed to the formation of THA^+/Br_3^- ion pairs in solution.[85] The disappearance of Br_2 may therefore primarily arise from the high stability of the TBA^+/Br_3^- ion pair, which delays its evaporation for times much longer than our 110 μs observation time.

We can make this argument quantitative by estimating the effective Br_2 solubility that would reduce its evaporation to 15% upon addition of 0.005 *m* TBABr to 6 m LiBr at 263 K. As calculated in the Appendix, the equilibrium constant for tight ion pairing via $Br_3^- + TBA^+ \rightleftharpoons TBA^+/Br_3^-$ must be at least 8000, which causes a 40-fold increase in the solubility of Br_2 in the absence of TBA^+. This enhanced solvation increases the predicted Br_2 residence time to ~1 s and decreases its evaporation to just 1% when the TBABr concentration is raised to 0.050 *m*, in accord with our inability to detect it. The high concentration of TBA^+ and Br^- at the surface makes it likely that Br_3^- is created near the surface and forms ion pairs with the segregated TBA^+ cations. However, this interfacial ion pair formation may not be essential. Even in the absence of interfacial TBA^+, the predicted 6 μs solvation time for Br_3^- allows these ions to diffuse ~400 Å and encounters on average five TBA^+ ions in the bulk of the 0.005 *m* solution before it evaporates as Br_2. Thus, Br_3^- ions created by N_2O_5 may be trapped by TBA^+ at or below the interfacial region.

■ CONCLUDING REMARKS

The N_2O_5 scattering experiments described here provide the first opportunity to explore the conversion of a reactant to product through collisions of a reactive gas with salty and surfactant-coated water microjets in vacuum. The reaction of N_2O_5 with Br^- in 6 *m* $LiBr/H_2O$ at 263 K generates evaporating Br_2, likely passing through the Br_3^- intermediate shown in Figure 1. For the 6 *m* Br^- solution used here, the $Br_2 + Br^- \rightleftharpoons Br_3^-$ equilibrium lengthens the average Br_2 residence time in solution from much less than 1−6 μs. This solvation time increases even further to potentially 1 s by the addition of 0.05 *m* TBA^+ ions, which strongly pair with Br_3^- ions.

DOI: 10.1021/acs.jpca.9b04225
J. Phys. Chem. A XXXX, XXX, XXX−XXX

The extended residence time of Br_2 in solution as Br_3^- may provide opportunities for other interfacial and bulk-phase reactions to proceed, including the bromination of double bonds and aromatic rings in surface-active species. Indeed, $TBABr_3$ is a standard reagent used to safely supply Br_2 for these reactions.[86] These studies may also be expanded to investigate other soluble ocean surfactants, including short-chain carboxylic acids and polysaccharides,[87] following characterization of their interfacial concentrations by high-energy SF_6 scattering. In this way, we hope to explore reactions of N_2O_5 and hypohalous acids as well,[37] with salty and surfactant solutions that interconvert dissolved and gaseous halogen species through gas−liquid oxidation−reduction reactions.

APPENDIX

Br_2 Residence Time and Evaporation Probability from the Microjet

To estimate the residence time of Br_2 molecules in 6 *m* LiBr/H_2O at 263 K in the absence and presence of TBABr, we first calculate its effective solubility and diffusivity. The solubility of Br_2 is enhanced by the reaction with Br^- to form Br_3^- via the reaction[43,70]

$$Br_2 + Br^- \rightleftharpoons Br_3^- \qquad K_{Br} = 16 \text{ at } 298 \text{ K}$$

Assuming that the activity coefficient of Br_2 is close to one and that the activity coefficients of Br_3^- and Br^- are similar, the effective solubility of Br_2 is given by

$$H_{eff} = \frac{[Br_2] + [Br_3^-]}{P_{Br_2}} = H_{phys}(1 + K_{Br}[Br^-]) \tag{A.1}$$

where $H_{phys} = [Br_2]/P_{Br_2}$ is the Henry's law physical solubility of Br_2 (equal to 0.77 M atm^{-1} at 298 K in pure water). Using the thermodynamic parameters of Liu and Margerum, we extrapolate to values of H_{phys} = 4.3 M atm^{-1}, K_{Br} = 16, and H_{eff} = 360 M atm^{-1} for 6 *m* LiBr at 263 K.[43,70] The formation of Br_3^- therefore enhances Br_2 solubility by 90-fold. The diffusivity of the dominant Br_3^- species in 6 *m* LiBr at 263 K was estimated by scaling its diffusion coefficient of 1.2×10^{-5} cm^2 s^{-1} in pure water at 298 K by the ratio of viscosities (5 cP in 6 *m* LiBr at 263 K vs 0.89 cP in pure water at 298 K) and temperatures to be $D = 2.4 \times 10^{-6}$ cm^2 s^{-1}.[45]

The characteristic residence time τ for Br_2 in solution in the form of Br_3^- can be roughly estimated by assuming that N_2O_5 is converted into Br_2 and Br_3^- in the near-interfacial region, effectively acting as a source of Br_2 deposition into solution. In this case,

$$\tau = D\left(\frac{4H_{eff}RT}{\alpha\bar{v}}\right)^2 \tag{A.2}$$

where T is the solution temperature, $\bar{v}$ is the mean speed of Br_2, and α is the effective entry probability, limited by N_2O_5 dissolution.[68,88,89] τ is the time for the outgoing flux of Br_2 molecules from a freshly exposed solution to rise to 57% of its maximum value at saturation. Gržinić et al. have measured $\alpha(N_2O_5) > 0.4$ at 298 K, and we set it equal to 1 at 263 and 240 K in this analysis.[66] Using the calculated values for H_{eff}, we find that Br_3^- formation extends the solvation time of Br_2 from much less than 1−6 μs for 6 *m* LiBr/H_2O.

We next calculate the Br_2 evaporation probability for this predicted 6 μs solvation time. The incident N_2O_5 beam strikes the jet over its entire length, and we observe Br_2 evaporation from t_{beg} = 90 μs at 2.6 mm to t_{end} = 200 μs at 5.9 mm when the jet is traveling at 30 m s^{-1}. We model the 35 μm diameter jet as a flat sheet because the diffusion depth over 200 μs is only 0.2 μm.[15] The fraction P_{Br_2} of evaporating Br_2 molecules is then calculated by integrating the outgoing Br_2 flux F by

$$P_{Br_2} = \frac{F(t_{beg} \text{ to } t_{end})}{(t_{end} - t_{beg})} = \frac{F(0 \text{ to } t_{end}) - F(0 \text{ to } t_{beg})}{(t_{end} - t_{beg})} \tag{A.3}$$

where

$$F(0 \text{ to } t) = t - \tau\left[\text{erfc}\left(\sqrt{\frac{t}{\tau}}\right)e^{t/\tau} + \frac{2}{\sqrt{\pi}}\sqrt{\frac{t}{\tau}} - 1\right] \tag{A.4}$$

is proportional to the Br_2 evaporation flux over time t.[88,89] Eqs A.3 and A.4 yield an evaporation probability of 0.87, implying that we measure a significant fraction of Br_2 produced by the reaction between N_2O_5 and Br^- over the short observation window.

This analysis can be extended to determine the increase in solubility of Br_2 upon adding 0.005 *m* TBABr to 6 *m* LiBr at 263 K. Under these conditions, we measure an 85% reduction in signal (Figure 12). The presence of TBA^+ increases H_{eff} through the reversible reaction $Br_3^- + TBA^+ \rightleftharpoons TBA^+/Br_3^-$, characterized by K_{TBA}. H_{eff} is therefore enhanced by

$$H_{eff} = \frac{[Br_2] + [Br_3^-] + [TBABr_3]}{P_{Br_2}} = H_{phys}(1 + K_{Br}[Br^-] + K_{Br}K_{TBA}[Br^-][TBA^+]) \tag{A.5}$$

We find that K_{TBA} must be near 8000 to force the Br_2 signal to drop to 15% of its value by addition of 0.005 *m* TBABr. This complexation increases H_{eff} by 40 and τ by 1600 to roughly 0.01 s. When the TBABr concentration is increased to 0.05 *m*, the same value of K_{TBA} causes τ to rise to 1 s and the Br_2 evaporation probability to drop to 1%, a low probability consistent with our inability to observe any Br_2. We assume here that TBA^+ does not itself catalyze the production of Br_2, as we have observed when THABr is added to 0.3 and 2.7 M NaBr/glycerol solutions.[38] If TBA^+ does enhance Br_2 production, then it must be captured for even longer times in solution as Br_3^- than we have estimated.

ASSOCIATED CONTENT

Supporting Information

The Supporting Information is available free of charge on the ACS Publications website at DOI: 10.1021/acs.jpca.9b04225.

Comparison of N_2O_5 and $CHCl_3$ TOF spectra for investigating imperfect MB fits in Figure 4 (PDF)

AUTHOR INFORMATION

Corresponding Authors

*E-mail: timothy.bertram@wisc.edu (T.H.B.).
*E-mail: gmnathan@wisc.edu (G.M.N.).

ORCID

Thomas B. Sobyra: 0000-0002-8891-3271
Helena Pliszka: 0000-0003-1563-0649
Timothy H. Bertram: 0000-0002-3026-7588
Gilbert M. Nathanson: 0000-0002-6921-6841

DOI: 10.1021/acs.jpca.9b04225
J. Phys. Chem. A XXXX, XXX, XXX−XXX

Notes

The authors declare no competing financial interest.

■ ACKNOWLEDGMENTS

We are grateful to the National Science Foundation for supporting this research via the Center for Aerosol Impacts on Chemistry of the Environment, a NSF Center for Chemical Innovation (NSF CHE 1801971). T.B.S. was supported by a NSF Graduate Research Fellowship (DGE-1256259). We also thank Sarah Quinn and Chi-Min Ni for assistance with the surface tension measurements, Pavel Jungwirth for permission to use the simulation snapshot in Figure 8 and Douglas Tobias and John Hemminger for permission to use the simulation snapshot in Figure 10, and Laura McCaslin for a close reading of the manuscript.

■ REFERENCES

(1) Faubel, M. Photoionization and Photodetachment. In *Photoionization and Photodetachment*, Ng, C., Ed.; World Scientific: New Jersey, 2000; Vol. *10A*, pp 634−690.

(2) Wilson, K. R.; Rude, B. S.; Smith, J.; Cappa, C.; Co, D. T.; Schaller, R. D.; Larsson, M.; Catalano, T.; Saykally, R. J. Investigation of Volatile Liquid Surfaces by Synchrotron X-ray Spectroscopy of Liquid Microjets. *Rev. Sci. Instrum.* **2004**, *75*, 725−736.

(3) Winter, B.; Faubel, M. Photoemission from Liquid Aqueous Solutions. *Chem. Rev.* **2006**, *106*, 1176−1211.

(4) Faust, J. A.; Nathanson, G. M. Microjets and Coated Wheels: Versatile Tools for Exploring Collisions and Reactions at Gas-Liquid Interfaces. *Chem. Soc. Rev.* **2016**, *45*, 3609−3620.

(5) Perrine, K. A.; Parry, K. M.; Stern, A. C.; Van Spyk, M. H. C.; Makowski, M. J.; Freites, J. A.; Winter, B.; Tobias, D. J.; Hemminger, J. C. Specific Cation Effects at Aqueous Solution-Vapor Interfaces: Surfactant-Like Behavior of Li^+ Revealed by Experiments and Simulations. *Proc. Natl. Acad. Sci. U.S.A.* **2017**, *114*, 13363−13368.

(6) Chen, L.; Chen, Z.; Li, Z.; Hu, J.; Tian, S. X. Time-Delayed Mass Spectrometry of the Low-Energy Electron Impact with a Liquid Beam Surface. *Rev. Sci. Instrum.* **2018**, *89*, 103102.

(7) Ryazanov, M.; Nesbitt, D. J. Quantum-State-Resolved Studies of Aqueous Evaporation Dynamics: NO Ejection from a Liquid Water Microjet. *J. Chem. Phys.* **2019**, *150*, 044201.

(8) Faubel, M.; Schlemmer, S.; Toennies, J. P. A Molecular Beam Study of the Evaporation of Water from a Liquid Jet. *Z. Phys. D: At., Mol. Clusters* **1988**, *10*, 269−277.

(9) Gladytz, T.; Abel, B.; Siefermann, K. R. Expansion Dynamics of Supercritical Water Probed by Picosecond Time-Resolved Photoelectron Spectroscopy. *Phys. Chem. Chem. Phys.* **2015**, *17*, 4926−4936.

(10) Faubel, M.; Kisters, T. Non-Equilibrium Molecular Evaporation of Carboxylic Acid Dimers. *Nature* **1989**, *339*, 527−529.

(11) Maselli, O. J.; Gascooke, J. R.; Lawrance, W. D.; Buntine, M. A. The Dynamics of Evaporation from a Liquid Surface. *Chem. Phys. Lett.* **2011**, *513*, 1−11.

(12) Hahn, C.; Kann, Z. R.; Faust, J. A.; Skinner, J. L.; Nathanson, G. M. Super-Maxwellian Helium Evaporation from Pure and Salty Water. *J. Chem. Phys.* **2016**, *144*, 044707.

(13) Lewis, T.; Faubel, M.; Winter, B.; Hemminger, J. C. CO_2 Capture in Amine-Based Aqueous Solution: Role of the Gas-Solution Interface. *Angew. Chem., Int. Ed. Engl.* **2011**, *50*, 10178−10181.

(14) Lee, M.-T.; Brown, M. A.; Kato, S.; Kleibert, A.; Turler, A.; Ammann, M. Competition between Organics and Bromide at the Aqueous Solution-Air Interface as seen from Ozone Uptake Kinetics and X-ray Photoelectron Spectroscopy. *J. Phys. Chem. A* **2015**, *119*, 4600−4608.

(15) Sobyra, T. B.; Melvin, M. P.; Nathanson, G. M. Liquid Microjet Measurements of the Entry of Organic Acids and Bases into Salty Water. *J. Phys. Chem. C* **2017**, *121*, 20911−20924.

(16) Frenzel, A.; Scheer, V.; Sikorski, R.; George, C.; Behnke, W.; Zetzsch, C. Heterogeneous Interconversion Reactions of $BrNO_2$, $ClNO_2$,Br_2, and Cl_2. *J. Phys. Chem. A* **1998**, *102*, 1329−1337.

(17) Schweitzer, F.; Mirabel, P.; George, C. Multiphase Chemistry of N_2O_5, $ClNO_2$, and $BrNO_2$. *J. Phys. Chem. A* **1998**, *102*, 3942−3952.

(18) Bertram, T. H.; Thornton, J. A. Toward a General Parameterization of N_2O_5 Reactivity on Aqueous Particles: the Competing Effects of Particle Liquid Water, Nitrate and Chloride. *Atmos. Chem. Phys.* **2009**, *9*, 8351−8363.

(19) Brown, S. S.; Stutz, J. Nighttime Radical Observations and Chemistry. *Chem. Soc. Rev.* **2012**, *41*, 6405−6447.

(20) Abbatt, J. P. D.; Lee, A. K. Y.; Thornton, J. A. Quantifying Trace Gas Uptake to Tropospheric Aerosol: Recent Advances and Remaining Challenges. *Chem. Soc. Rev.* **2012**, *41*, 6555−6581.

(21) McDuffie, E. E.; Fibiger, D. L.; Dubé, W. P.; Lopez-Hilfiker, F.; Lee, B. H.; Jaeglé, L.; Guo, H. Y.; Weber, R. J.; Reeves, J. M.; Weinheimer, A. J.; et al. $ClNO_2$ Yields From Aircraft Measurements During the 2015 WINTER Campaign and Critical Evaluation of the Current Parameterization. *J. Geophys. Res.: Atmos.* **2018**, *123*, 12994−13015.

(22) Chang, W. L.; Bhave, P. V.; Brown, S. S.; Riemer, N.; Stutz, J.; Dabdub, D. Heterogeneous Atmospheric Chemistry, Ambient Measurements, and Model Calculations of N_2O_5: A Review. *Aerosol Sci. Technol.* **2011**, *45*, 665−695.

(23) N_2O_5, $ClNO_2$, HNO_3, and likely $BrNO_2$ ionize predominantly at NO_2^+, yielding no ions (N_2O_5) or very few ions (HNO_3) at the parent mass upon electron impact ionization. See refs.[24,26]

(24) Hoffman, R. C.; Gebel, M. E.; Fox, B. S.; Finlayson-Pitts, B. J. Knudsen Cell Studies of the Reactions of N_2O_5 and $ClONO_2$ with NaCl: Development and Application of a Model for Estimating Available Surface Areas and Corrected Uptake Coefficients. *Phys. Chem. Chem. Phys.* **2003**, *5*, 1780−1789.

(25) O'Connor, C. S. S.; Jones, N. C.; O'Neale, K.; Price, S. D. Electron-Impact Ionization of Dinitrogen Pentoxide. *Int. J. Mass Spectrom.* **1996**, *154*, 203−211.

(26) O'Connor, C. S. S.; Jones, N. C.; Price, S. D. Electron-Impact Ionization of Nitric Acid. *Int. J. Mass Spectrom.* **1997**, *163*, 131−139.

(27) Roberts, J. M.; Osthoff, H. D.; Brown, S. S.; Ravishankara, A. R.; Coffman, D.; Quinn, P.; Bates, T. Laboratory Studies of Products of N_2O_5 Uptake on Cl^- Containing Substrates. *Geophys. Res. Lett.* **2009**, *36*, L20808.

(28) Puar, M. S. Nucleophilic Reactivities of the Halide Anions. *J. Chem. Educ.* **1970**, *47*, 473−474.

(29) Anslyn, E. V.; Dougherty, E. A. *Modern Physical Organic Chemistry*; University Science Books: Herndon, VA, 2006; Chapter 8.

(30) Lopez-Hilfiker, F. D.; Constantin, K.; Kercher, J. P.; Thornton, J. A. Temperature Dependent Halogen Activation by N_2O_5 Reactions on Halide-Doped Ice Surfaces. *Atmos. Chem. Phys.* **2012**, *12*, 5237−5247.

(31) McNamara, J. P.; Hillier, I. H. Exploration of the Atmospheric Reactivity of N_2O_5 and HCl in Small Water Clusters Using Electronic Structure Methods. *Phys. Chem. Chem. Phys.* **2000**, *2*, 2503−2509.

(32) Kelleher, P. J.; Menges, F. S.; DePalma, J. W.; Denton, J. K.; Johnson, M. A.; Weddle, G. H.; Hirshberg, B.; Gerber, R. B. Trapping and Structural Characterization of the $XNO_2{\cdot}NO_3^-$ (X = CI, Br, I) Exit Channel Complexes in the Water-Mediated X^- + N_2O_5 Reactions with Cryogenic Vibrational Spectroscopy. *J. Phys. Chem. Lett.* **2017**, *8*, 4710−4715.

(33) McCaslin, L. M.; Johnson, M. A.; Gerber, R. B. Mechanisms and Competition of Halide Substitution and Hydrolysis in Reactions of N_2O_5 and Seawater. *Sci. Adv.* **2019**, *5*, No. eaav6503.

(34) Hirshberg, B.; Rossich Molina, E.; Götz, A. W.; Hammerich, A. D.; Nathanson, G. M.; Bertram, T. H.; Johnson, M. A.; Gerber, R. B. N_2O_5 at Water Surfaces: Binding Forces, Charge Separation, Energy Accommodation, and Atmospheric Implications. *Phys. Chem. Chem. Phys.* **2018**, *20*, 17961−17976.

DOI: 10.1021/acs.jpca.9b04225
J. Phys. Chem. A XXXX, XXX, XXX−XXX

(35) For a report of Cl_2 formation, see Roberts, J. M.; Osthoff, H. D.; Brown, S. S.; Ravishankara, A. R. N_2O_5 Oxidizes Chloride to Cl_2 in Acidic Atmospheric Aerosol. *Science* **2008**, *321*, 1059.

(36) Talukdar, R. K.; Burkholder, J. B.; Roberts, J. M.; Portmann, R. W.; Ravishankara, A. R. Heterogeneous Interaction of N_2O_5 with HCl Doped H_2SO_4 under Stratospheric Conditions: $ClNO_2$ and Cl_2 Yields. *J. Phys. Chem. A* **2012**, *116*, 6003−6014.

(37) Simpson, W. R.; Brown, S. S.; Saiz-Lopez, A.; Thornton, J. A.; Von Glasow, R. Tropospheric Halogen Chemistry: Sources, Cycling, and Impacts. *Chem. Rev.* **2015**, *115*, 4035−4062.

(38) Shaloski, M. A.; Gord, J. R.; Staudt, S.; Quinn, S. L.; Bertram, T. H.; Nathanson, G. M. Reactions of N_2O_5 with Salty and Surfactant-Coated Glycerol: Interfacial Conversion of Br^- to Br_2 Mediated by Alkylammonium Cations. *J. Phys. Chem. A* **2017**, *121*, 3708−3719.

(39) Reference 40 reports that $\Delta_f G°(BrNO_2(g))$ is +96 kJ mol^{-1}, while ref 41 reports that the solubility of $BrNO_2$ in water is 0.3 M atm^{-1} at 298 K. These values result in a reaction free energy of −23 kJ mol^{-1} for $Br^-(aq) + BrNO_2(aq) \rightleftharpoons Br_2(aq) + NO_2^-(aq)$. The analogous $\Delta_f G°(ClNO_2(g))$ is +54.4 kJ mol^{-1} and its solubility is reported as 0.04 M atm^{-1}, resulting in a reaction free energy of +42 kJ mol^{-1} for $Cl^-(aq) + ClNO_2(aq) \rightleftharpoons Cl_2(aq) + NO_2^-(aq)$.

(40) Kreutter, K. D.; Nicovich, J. M.; Wine, P. H. Kinetics and Thermochemistry of the $Br(^2P_{3/2}) + NO_2$ Association Reaction. *J. Phys. Chem.* **1991**, *95*, 4020−4028.

(41) Sander, R. Compilation of Henry's Law Constants (Version 4.0) for Water as Solvent. *Atmos. Chem. Phys.* **2015**, *15*, 4399−4981.

(42) Finlayson-Pitts, B. J.; Livingston, F. E.; Berko, H. N. Synthesis and Identification by Infrared Spectroscopy of Gaseous Nitryl Bromide, $BrNO_2$. *J. Phys. Chem.* **1989**, *93*, 4397−4400.

(43) Liu, Q.; Margerum, D. W. Equilibrium and Kinetics of Bromine Chloride Hydrolysis. *Environ. Sci. Technol.* **2001**, *35*, 1127−1133.

(44) Pátek, J.; Klomfar, J. Solid−Liquid Phase Equilibrium in the Systems of LiBr−H_2O and LiCl−H_2O. *Fluid Phase Equilib.* **2006**, *250*, 138−149.

(45) Wimby, J. M.; Berntsson, T. S. Viscosity and Density of Aqueous Solutions of LiBr, LiCl, $ZnBr_2$, $CaCl_2$, and $LiNO_3$, 1, Single Salt Solutions. *J. Chem. Eng. Data* **1994**, *39*, 68−72.

(46) Liu, W. T.; Tang, W.; Niiler, P. P. Humidity Profiles over the Ocean. *J. Clim.* **1991**, *4*, 1023−1034.

(47) Laskina, O.; Morris, H. S.; Grandquist, J. R.; Qin, Z.; Stone, E. A.; Tivanski, A. V.; Grassian, V. H. Size Matters in the Water Uptake and Hygroscopic Growth of Atmospherically Relevant Multicomponent Aerosol Particles. *J. Phys. Chem. A* **2015**, *119*, 4489−4497.

(48) Bertram, T. H.; Cochran, R. E.; Grassian, V. H.; Stone, E. A. Sea Spray Aerosol Chemical Composition: Elemental and Molecular Mimics for Laboratory Studies of Heterogeneous and Multiphase Reactions. *Chem. Soc. Rev.* **2018**, *47*, 2374−2400.

(49) Davidson, J. A.; Viggiano, A. A.; Howard, C. J.; Dotan, I.; Fehsenfeld, F. C.; Albritton, D. L.; Ferguson, E. E. Rate Constants for the Reactions of O_2^+, NO_2^+, NO^+, H_3O^+, CO_3^-, NO_2^-, and Halide Ions with N_2O_5 at 300 K. *J. Chem. Phys.* **1978**, *68*, 2085−2087.

(50) Osthoff, H. D.; Pilling, M. J.; Ravishankara, A. R.; Brown, S. S. Temperature Dependence of the NO_3 Absorption Cross-Section Above 298 K and Determination of the Equilibrium Constant for $NO_3 + NO_2 \leftrightarrow N_2O_5$ at Atmospherically Relevant Conditions. *Phys. Chem. Chem. Phys.* **2007**, *9*, 5785.

(51) Seisel, S.; Caloz, F.; Fenter, F. F.; van den Bergh, H.; Rossi, M. J. The Heterogeneous Reaction of NO_3 with NaCl and KBr: A Nonphotolytic Source of Halogen Atoms. *Geophys. Res. Lett.* **1997**, *24*, 2757−2760.

(52) Joshipura, K. N.; Gangopadhyay, S.; Vaishnav, B. G. Electron Scattering and Ionization of NO, N_2O, NO_2, NO_3 and N_2O_5 Molecules: Theoretical Cross Sections. *J. Phys. B: At., Mol. Opt. Phys.* **2007**, *40*, 199−210.

(53) The Ar−H_2O collision probability N_{coll} can be estimated from the 30 $Å^2$ cross section (ref 54), 35 μm jet diameter, 7 mm jet length before breakup, and 43 mm distance from the jet to the first aperture. According to eq 5 of ref 4, the fraction of Ar atoms that do not collide is $\exp(-N_{coll})$, which is 0.25 for 2.1 Torr vapor pressure at 263 K and 0.75 for 0.4 Torr at 240 K. Figure 3a shows only modest deviations from a Maxwell−Boltzmann distribution, implying that eq 5 of ref 4 overestimates N_{coll}.

(54) Vanfleteren, T.; Földes, T.; Herman, M.; Liévin, J.; Loreau, J.; Coudert, L. H. Experimental and Theoretical Investigations of H_2O-Ar. *J. Chem. Phys.* **2017**, *147*, 014302.

(55) King, D. A.; Wells, M. G. Molecular Beam Investigation of Adsorption Kinetics on Bulk Metal Targets: Nitrogen on Tungsten. *Surf. Sci.* **1972**, *29*, 454−482.

(56) Morris, J. R.; Behr, P.; Antman, M. D.; Ringeisen, B. R.; Splan, J.; Nathanson, G. M. Molecular Beam Scattering from Supercooled Sulfuric Acid: Collisions of HCl, HBr, and HNO_3 with 70 wt% D_2SO_4. *J. Phys. Chem. A* **2000**, *104*, 6738−6751.

(57) Ringeisen, B. R.; Muenter, A. H.; Nathanson, G. M. Collisions of HCl, DCl, and HBr with Liquid Glycerol: Gas Uptake, D → H Exchange, and Solution Thermodynamics. *J. Phys. Chem. B* **2002**, *106*, 4988−4998.

(58) Vieceli, J.; Roeselová, M.; Potter, N.; Dang, L. X.; Garrett, B. C.; Tobias, D. J. Molecular Dynamics Simulations of Atmospheric Oxidants at the Air-Water Interface: Solvation and Accommodation of OH and O_3. *J. Phys. Chem. B* **2005**, *109*, 15876−15892.

(59) Romero Lejonthun, L. S. E.; Andersson, P. U.; Hallquist, M.; Thomson, E. S.; Pettersson, J. B. C. Interactions of N_2O_5 and Related Nitrogen Oxides with Ice Surfaces: Desorption Kinetics and Collision Dynamics. *J. Phys. Chem. B* **2014**, *118*, 13427−13434.

(60) Hoffman, C. H.; Nesbitt, D. J. Quantum State Resolved 3D Velocity Map Imaging of Surface-Scattered Molecules: Incident Energy Effects in HCl + Self-Assembled Monolayer Collisions. *J. Phys. Chem. C* **2016**, *120*, 16687−16698.

(61) HNO_3 reactive uptake has been measured in three studies to be >0.2 at 298 K (ref 62), equal to 0.15 at 273 and predicted to be 0.49 at 240 K (ref 63), and most recently by ^{13}N-labeled HNO_3 to be 0.50 ± 0.20 at 298 K (ref 64). On the basis of this latter measurement, and the probable increase in entry as the temperature drops, we assume that HNO_3 dissolves on nearly every collision into 8 m LiBr at 240 K. This is also in accord with our own measurements (refs 15,56), which show that formic acid dissolves in nearly every collision with 8 m LiBr at 253 K and that HNO_3 does as well in 70 wt % D_2SO_4 at 213 K. Our preliminary measurements of HNO_3 collisions with 8 m LiBr at 240 K confirm an uptake near one.

(62) Abbatt, J. P. D.; Waschewsky, G. C. G. Heterogeneous Interactions of HOBr, HNO_3, O_3, and NO_2 with Deliquescent NaCl Aerosols at Room Temperature. *J. Phys. Chem. A* **1998**, *102*, 3719−3725.

(63) Davidovits, P.; Kolb, C. E.; Williams, L. R.; Jayne, J. T.; Worsnop, D. R. Update 1 of: Mass Accommodation and Chemical Reactions at Gas−Liquid Interfaces. *Chem. Rev.* **2011**, *111*, PR76−PR109.

(64) Guimbaud, C.; Arens, F.; Gutzwiller, L.; Gaggeler, H. W.; Ammann, M. Uptake of HNO_3 to Deliquescent Sea-Salt Particles: A Study Using the Short-Lived Radioactive Isotope Tracer ^{13}N. *Atmos. Chem. Phys.* **2002**, *2*, 249−257.

(65) Robinson, G. N.; Worsnop, D. R.; Jayne, J. T.; Kolb, C. E.; Davidovits, P. Heterogeneous Uptake of $ClONO_2$ and N_2O_5 by Sulfuric Acid Solutions. *J. Geophys. Res.: Atmos.* **1997**, *102*, 3583−3601.

(66) Gržinić, G.; Bartels-Rausch, T.; Turler, A.; Ammann, M. Efficient Bulk Mass Accommodation and Dissociation of N_2O_5 in Neutral Aqueous Aerosol. *Atmos. Chem. Phys.* **2017**, *17*, 6493−6502.

(67) Ringeisen, B. R.; Muenter, A. H.; Nathanson, G. M. Collisions of DCl with Liquid Glycerol: Evidence for Rapid, Near-Interfacial D → H Exchange and Desorption. *J. Phys. Chem. B* **2002**, *106*, 4999−5010.

(68) Dempsey, L. P.; Faust, J. A.; Nathanson, G. M. Near-Interfacial Halogen Atom Exchange in Collisions of Cl_2 with 2.7 M NaBr-Glycerol. *J. Phys. Chem. B* **2012**, *116*, 12306−12318.

(69) Langlois, G. G.; Li, W.; Gibson, K. D.; Sibener, S. J. Capture of Hyperthermal CO_2 by Amorphous Water Ice via Molecular Embedding. *J. Phys. Chem. A* **2015**, *119*, 12238−12244.

DOI: 10.1021/acs.jpca.9b04225
J. Phys. Chem. A XXXX, XXX, XXX−XXX

(70) Bartlett, W. P.; Margerum, D. W. Temperature Dependencies of the Henry's Law Constant and the Aqueous Phase Dissociation Constant of Bromine Chloride. *Environ. Sci. Technol.* **1999**, *33*, 3410−3414.
(71) Cussler, E. L. *Diffusion: Mass Transfer in Fluid Systems*, 2nd ed.; Cambridge University Press: New York, 1997.
(72) Barnes, G.; Gentle, I. *Interfacial Science: An Introduction*, 2nd ed.; Oxford University Press: Oxford, U.K., 2011; Chapter 3.
(73) Marcus, Y. Tetraalkylammonium Ions in Aqueous and Non-Aqueous Solutions. *J. Solution Chem.* **2008**, *37*, 1071−1098.
(74) Kaganer, V. M.; Möhwald, H.; Dutta, P. Structure and Phase Transitions in Langmuir Monolayers. *Rev. Mod. Phys.* **1999**, *71*, 779−819.
(75) Winter, B.; Weber, R.; Schmidt, P. M.; Hertel, I. V.; Faubel, M.; Vrbka, L.; Jungwirth, P. Molecular Structure of Surface-Active Salt Solutions: Photoelectron Spectroscopy and Molecular Dynamics Simulations of Aqueous Tetrabutylammonium Iodide. *J. Phys. Chem. B* **2004**, *108*, 14558−14564.
(76) Krisch, M. J.; D'Auria, R.; Brown, M. A.; Tobias, D. J.; Hemminger, C.; Ammann, M.; Starr, D. E.; Bluhm, H. The Effect of an Organic Surfactant on the Liquid-Vapor Interface of an Electrolyte Solution. *J. Phys. Chem. C* **2007**, *111*, 13497−13509.
(77) Grimmelmann, E. K.; Tully, J. C.; Cardillo, M. J. Hard-Cube Model Analysis of Gas-Surface Energy Accommodation. *J. Chem. Phys.* **1980**, *72*, 1039−1043.
(78) Lawrence, J. R.; Glass, S. V.; Nathanson, G. M. Evaporation of Water through Butanol Films at the Surface of Supercooled Sulfuric Acid. *J. Phys. Chem. A* **2005**, *109*, 7449−7457.
(79) Prosser, A. J.; Franses, E. I. Adsorption and Surface Tension of Ionic Surfactants at the Air−Water Interface: Review and Evaluation of Equilibrium Models. *Colloids Surf., A* **2001**, *178*, 1−40.
(80) Kim, H.; Revzin, A.; Gosting, L. J. Diffusion Coefficients of Tetrabutylammonium Halides in Water at 25 °C. *J. Phys. Chem.* **1973**, *77*, 2567−2570.
(81) Hao, L.; Leaist, D. G. Binary Mutual Diffusion Coefficients of Aqueous Alcohols. Methanol to 1-Heptanol. *J. Chem. Eng. Data* **1996**, *41*, 210−213.
(82) Thornton, J. A.; Abbatt, J. P. D. N_2O_5 Reaction on Submicron Sea Salt Aerosol: Kinetics, Products, and the Effect of Surface Active Organics. *J. Phys. Chem. A* **2005**, *109*, 10004−10012.
(83) Park, S.-C.; Burden, D. K.; Nathanson, G. M. The Inhibition of N_2O_5 Hydrolysis in Sulfuric Acid by 1-Butanol and 1-Hexanol Surfactant Coatings. *J. Phys. Chem. A* **2007**, *111*, 2921−2929.
(84) For contrary results involving Br^- at the dodecanol−water interface, see discussion in ref 76 and in Onorato, R. M.; Otten, D. E.; Saykally, R. J. Measurement of Bromide Ion Affinities for the Air/Water and Dodecanol/Water Interfaces at Molar Concentrations by UV Second Harmonic Generation Spectroscopy. *J. Phys. Chem. C* **2010**, *114*, 13746−13751.
(85) Faust, J. A.; Dempsey, L. P.; Nathanson, G. M. Surfactant-Promoted Reactions of Cl_2 and Br_2 with Br^- in Glycerol. *J. Phys. Chem. B* **2013**, *117*, 12602−12612.
(86) Saikia, I.; Borah, A. J.; Phukan, P. Use of Bromine and Bromo-organic Compounds in Organic Synthesis. *Chem. Rev.* **2016**, *116*, 6837−7042.
(87) Cochran, R. E.; Laskina, O.; Trueblood, J. V.; Estillore, A. D.; Morris, H. S.; Jayarathne, T.; Sultana, C. M.; Lee, C.; Lin, P.; Laskin, J.; et al. Molecular Diversity of Sea Spray Aerosol Particles: Impact of Ocean Biology on Particle Composition and Hygroscopicity. *Chem* **2017**, *2*, 655−667.
(88) Crank, J. *The Mathematics of Diffusion*, 2nd ed.; Clarendon Press: Oxford, U.K., 1975; Chapters 3 and 5.
(89) Shi, Q.; Davidovits, P.; Jayne, J. T.; Worsnop, D. R.; Kolb, C. E. Uptake of Gas-Phase Ammonia. 1. Uptake by Aqueous Surfaces as a Function of pH. *J. Phys. Chem. A* **1999**, *103*, 8812−8823.

DOI: 10.1021/acs.jpca.9b04225
J. Phys. Chem. A XXXX, XXX, XXX−XXX